DEEP LEARNING BASED AUTOMATIC GROUNDING LINE DELINEATION IN DINSAR INTERFEROGRAMS

Sindhu Ramanath Tarekere[1], Lukas Krieger[1], Konrad Heidler[2], Dana Floricioiu[1]

[1]SAR Signal Processing, German Aerospace Center (DLR), Oberpfaffenhofen
[2]Data Science in Earth Observation, Technical University of Munich

Grounding line delineation in DInSAR interferograms

- The manual delineation of one DInSAR interferogram takes several minutes
- This is impractical given the volume of SAR acquisitions (from 1992 to present)
- Current GL datasets contain manually drawn lines → not up to date with available SAR acquisitions

Existing solution:

- Deep neural network based GL delineation algorithm by (Mohajerani et al., 2021)

Our solution:

- Uses manual delineations to train a convolutional neural network
- Explores the importance of several features towards grounding line delineation

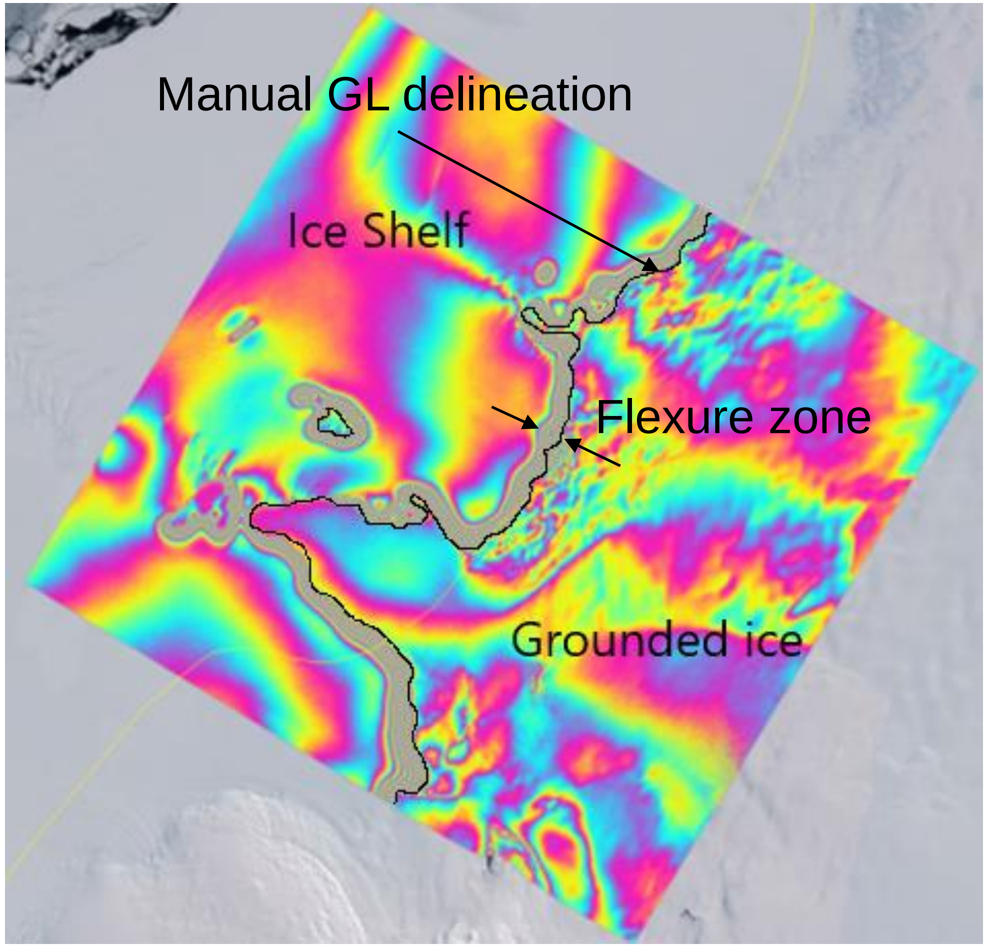

Mohajerani, Y., Jeong, S., Scheuchl, B., Velicogna, I., Rignot, E., & Milillo, P. (2021). Automatic delineation of glacier grounding lines in differential interferometric synthetic-aperture radar data using deep learning. *Scientific Reports*, *11*(1), 4992. https://doi.org/10.1038/s41598-021-84309-3

Antarctic SAR coverage of grounding zones

Sentinel-1 A/B constellation (6 days repeat) 2016 - 2021

Sentinel-1 (12-days repeat) 2014 - ongoing

TerraSAR-X (11-days repeat) 2009 - 2022

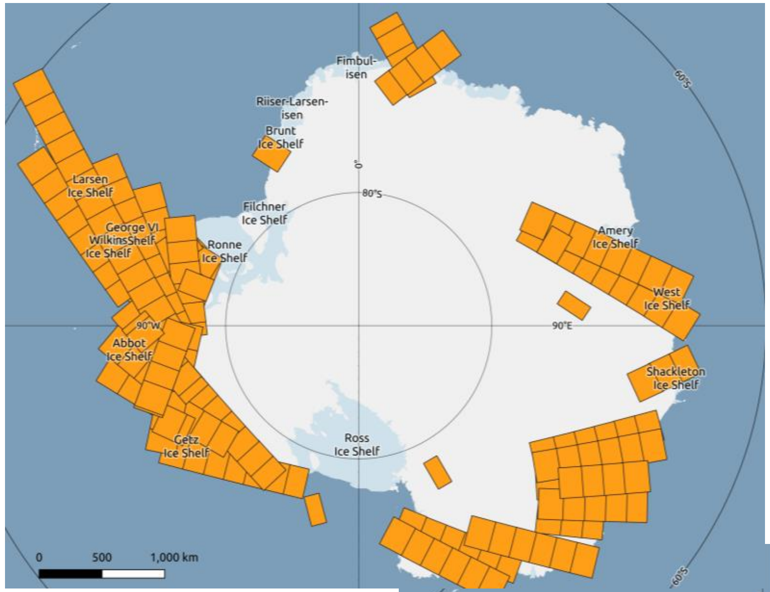

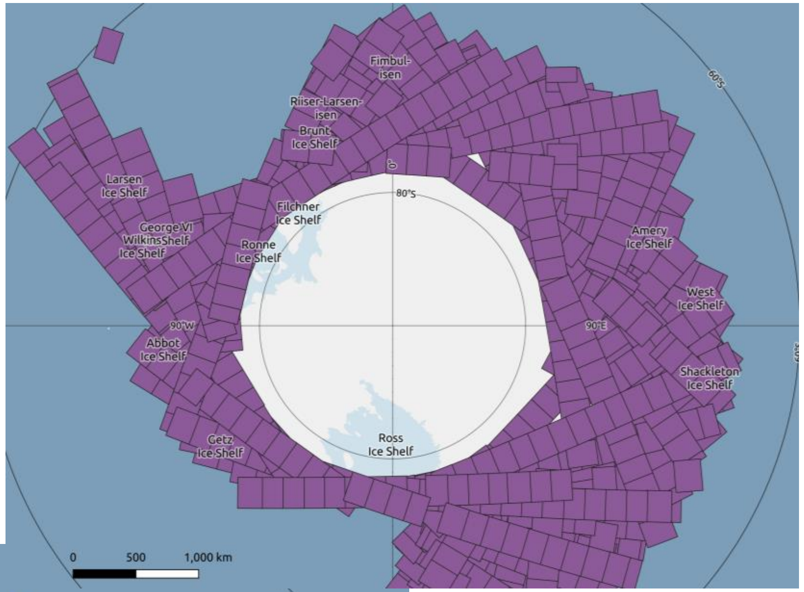

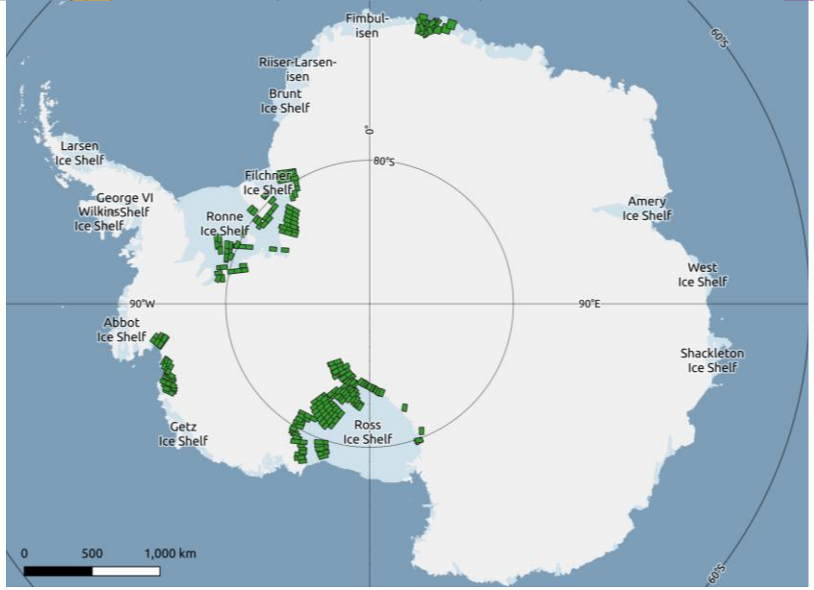

- No Sentinel-1 coverage south of 75°S (pole hole)
- The loss of S1-B increases temporal baseline to 12 days -> loss of coherence
- TerraSAR-X left looking mode covers south of 81°S (Ross and Ronne-Filchner Ice Shelves)

Training dataset: ground truth labels

Manually delineated GLs from Antarctic Ice Sheet climate change initiative (AIS_cci) Grounding Line Location product

Satellite (Imaging mode)	Temporal extent [years]	Repeat cycle [days]	No. of DInSAR interferograms
Sentinel 1 A/B (IW TOPS)	2014 – 2021	6, 12	199
ERS 1/2 (SM)	1992 – 1996	1, 3	123
TerraSAR-X (SM)	2012 – 2018	11	107

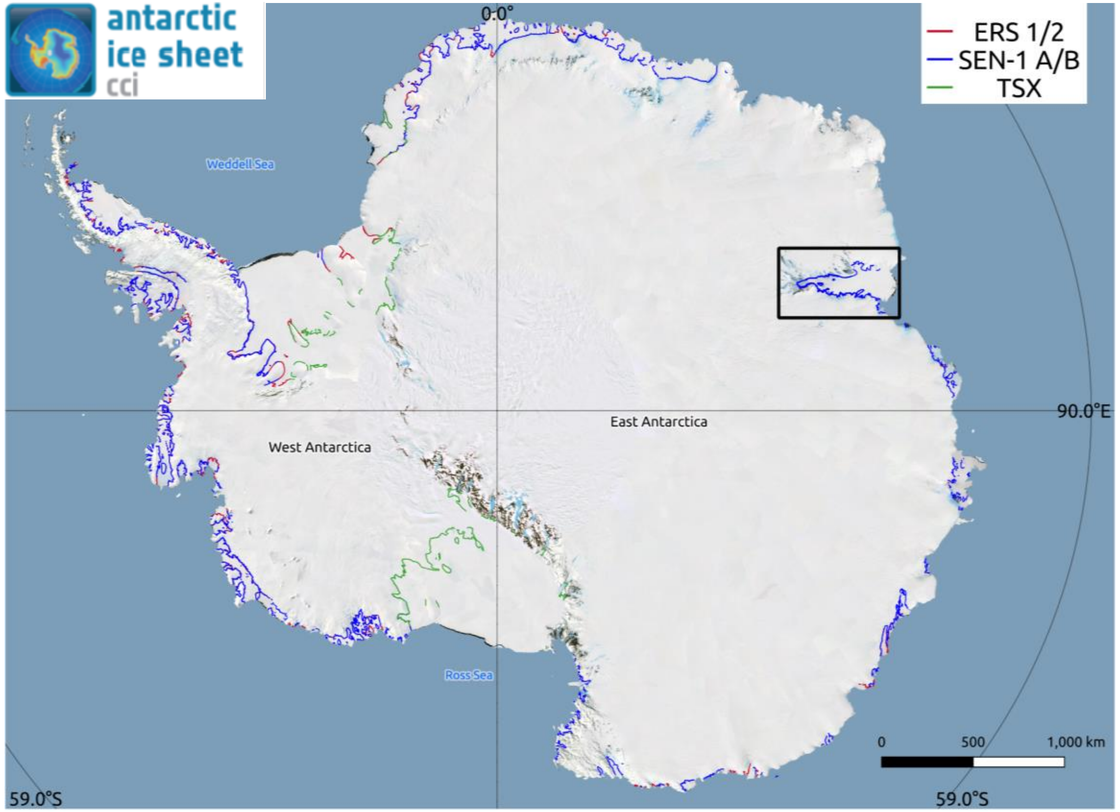

Groh., A. (2021) Product user guide (PUG) for the Antarctic_Ice_Sheet_cci project of ESA's Climate Change Initiative, version 1.0, https://climate.esa.int/media/documents/ST-UL-ESA-AISCCI-PUG-0001.pdf

Training dataset: input features

Feature	Dataset	Resolution	Temporal coverage [years]
DInSAR interferograms	AIS_cci	S1: 0.00043° ERS 1/2: 0.00055° TSX: 0.00016°	1992 - 2021
DEM	TanDEM-X PolarDEM	90 m	April 2013 – Oct 2014 July 2016 – Sept 2017
Ice velocity	ENVEO IT	200 m	2014 - 2021

Dynamic

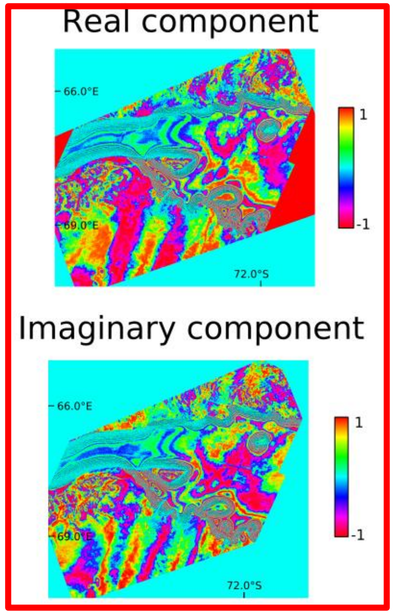

Temporally/Spatially restricted

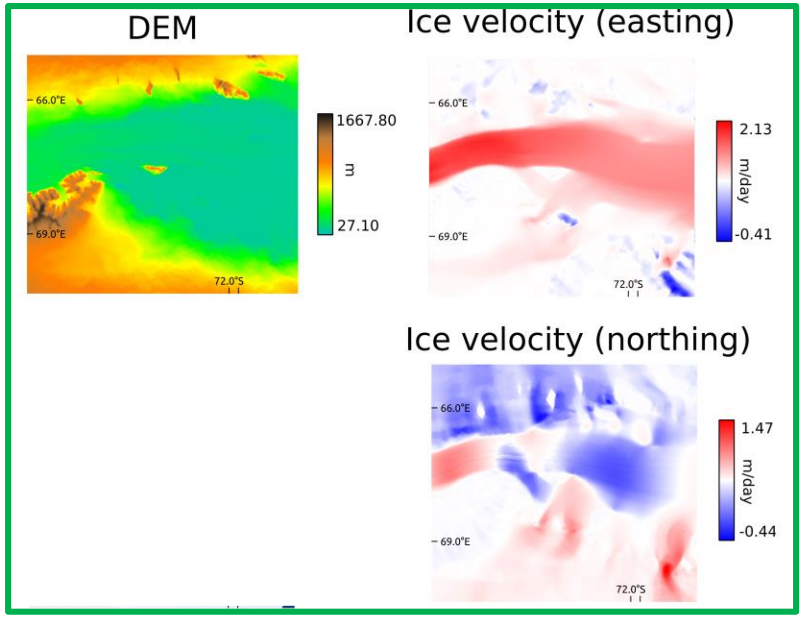

Groh., A. (2021) Product user guide (PUG) for the Antarctic_Ice_Sheet_cci project of ESA's Climate Change Initiative, version 1.0, https://climate.esa.int/media/documents/ST-UL-ESA-AISCCI-PUG-0001.pdf
Huber., M (2020) TanDEM-X PolarDEM Product Description, prepared by German Remote Sensing Data Center (DFD) and Earth Observation Center
Padman., L et al. (2002) Improving Antarctic tide models by assimilation of ICESat laser altimetry over ice shelves, *Geophysical Research Letters*, 35(22)
Nagler., T et al., (2015) The Sentinel-1 mission: New opportunities for ice sheet observations, *Remote Sensing*, vol. 7, no.7, pp.9371-9389

Automatic delineation pipeline

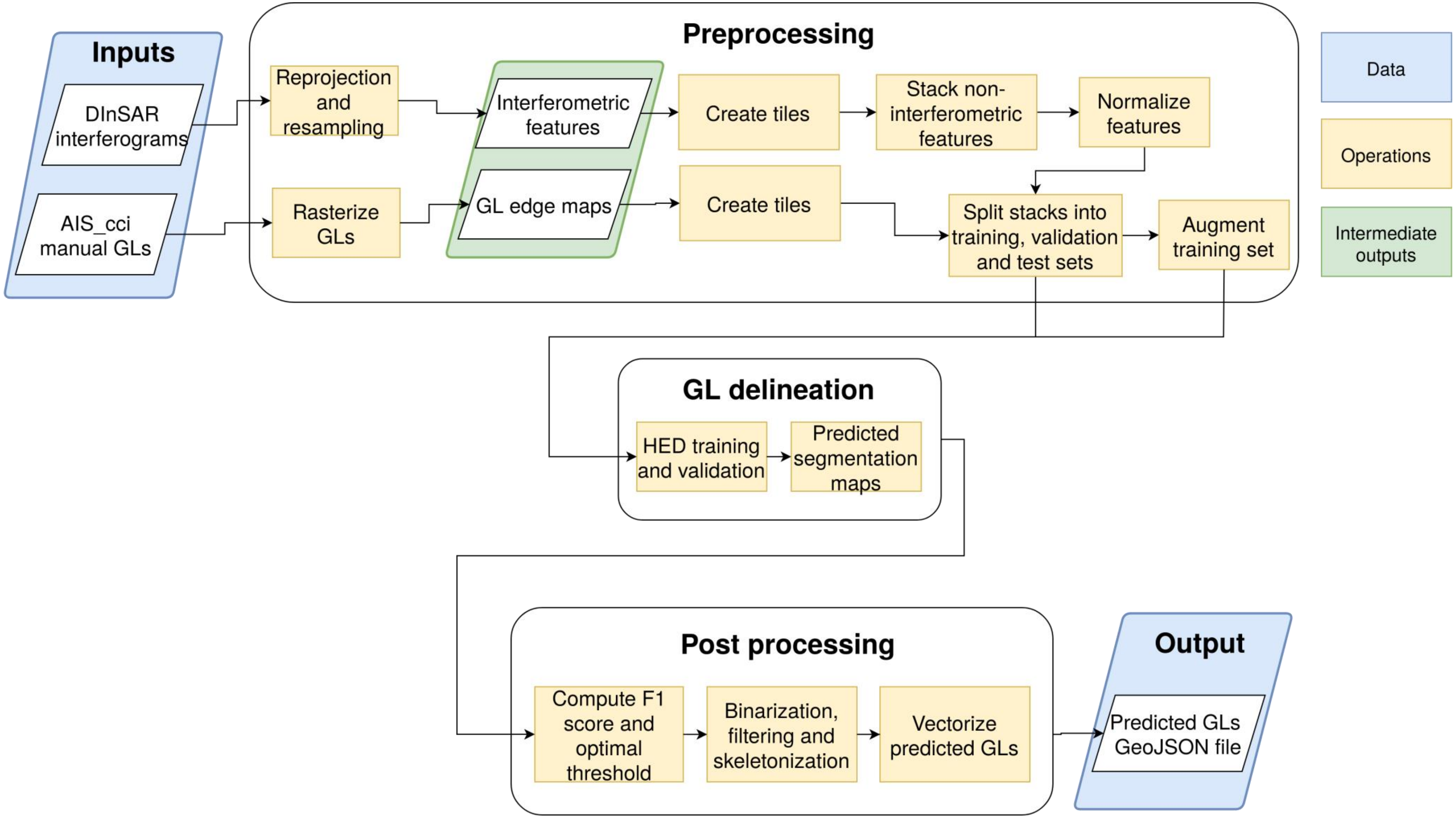

Preprocessing

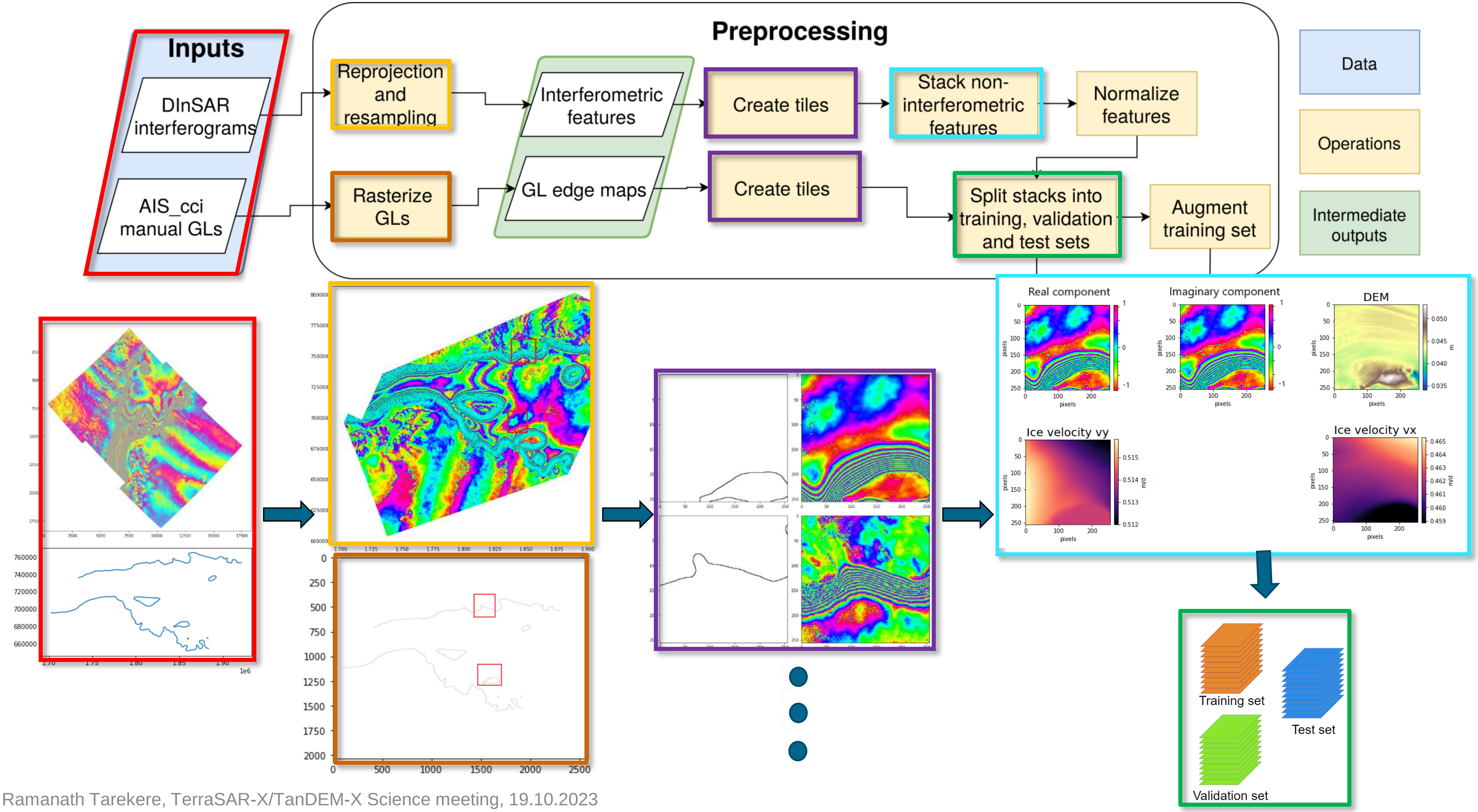

Inputs

DInSAR interferograms

AIS_cci manual GLs

Preprocessing

Reprojection and resampling

Rasterize GLs

Interferometric features

GL edge maps

Create tiles

Create tiles

Stack non-interferometric features

Normalize features

Split stacks into training, validation and test sets

Augment training set

Data

Operations

Intermediate outputs

Neural network training procedure

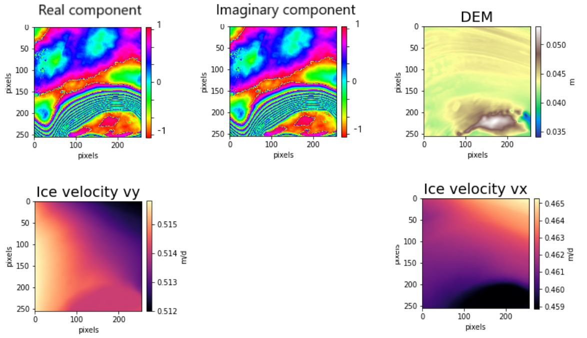

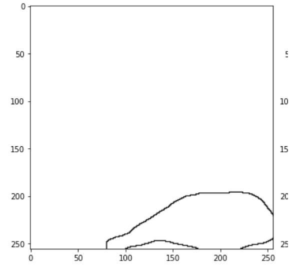

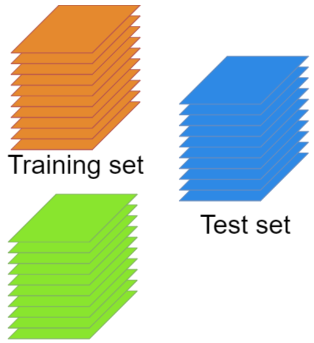

Validation set

Holistically-Nested Edge Detection

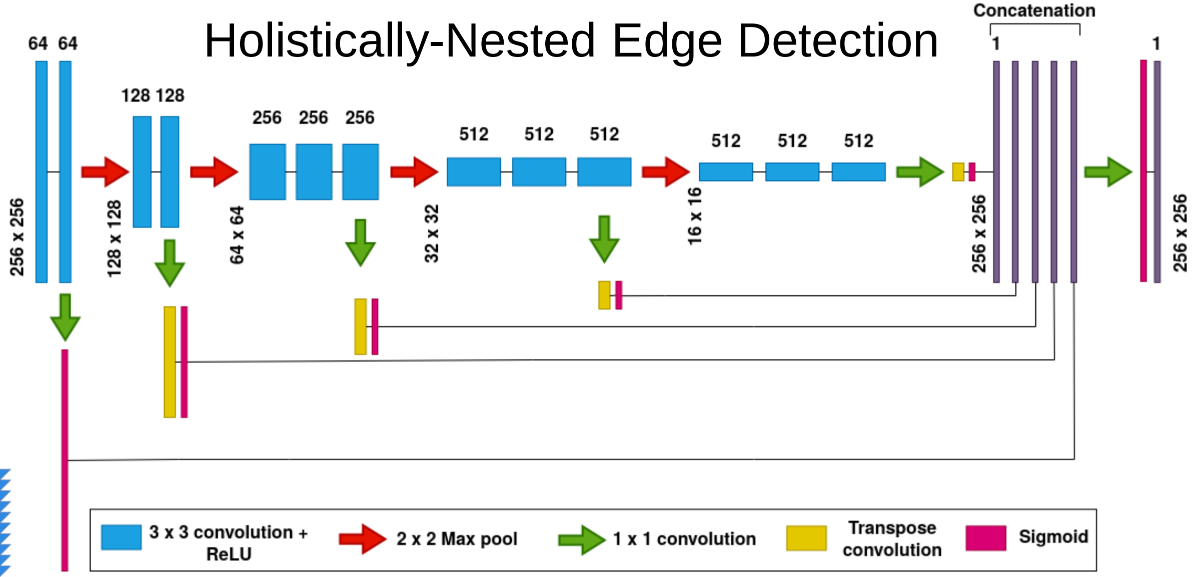

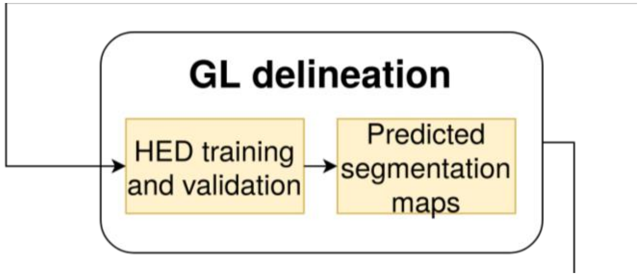

GL delineation

HED training and validation → Predicted segmentation maps

Segmentation maps

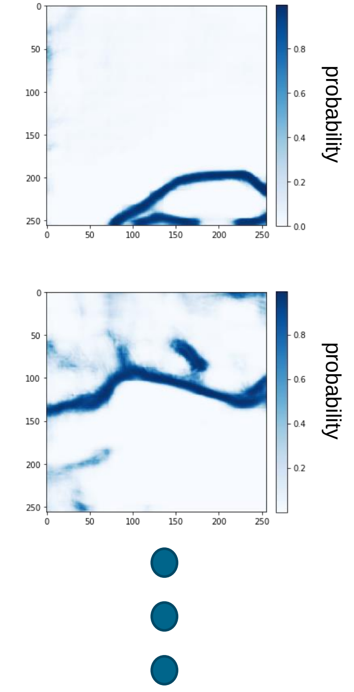

Xie, S., & Tu, Z. (2015). Holistically-nested edge detection. In Proceedings of the IEEE international conference on computer vision (pp. 1395-1403)

Postprocessing

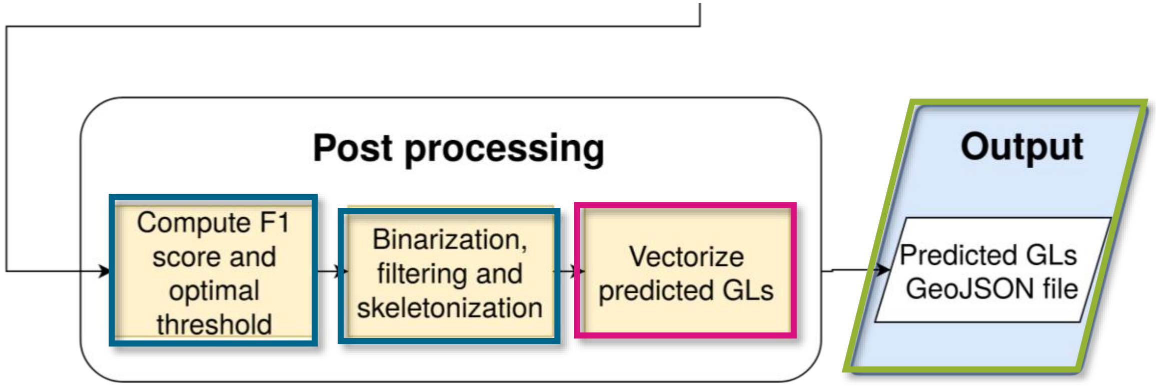

Post processing

Compute F1 score and optimal threshold

Binarization, filtering and skeletonization

Vectorize predicted GLs

Output

Predicted GLs GeoJSON file

Segmentation maps

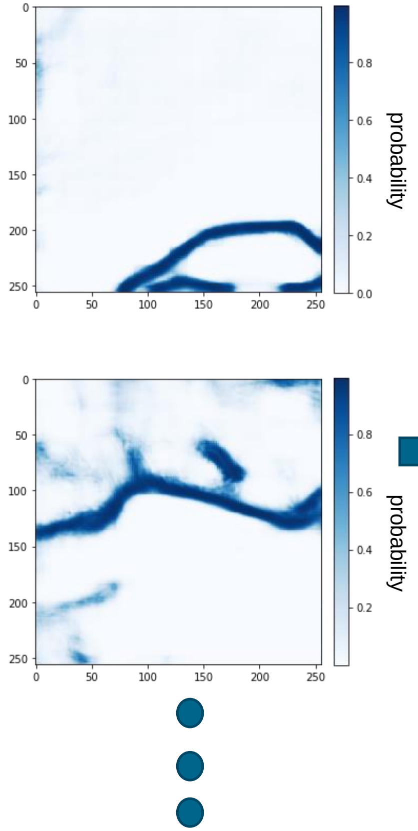

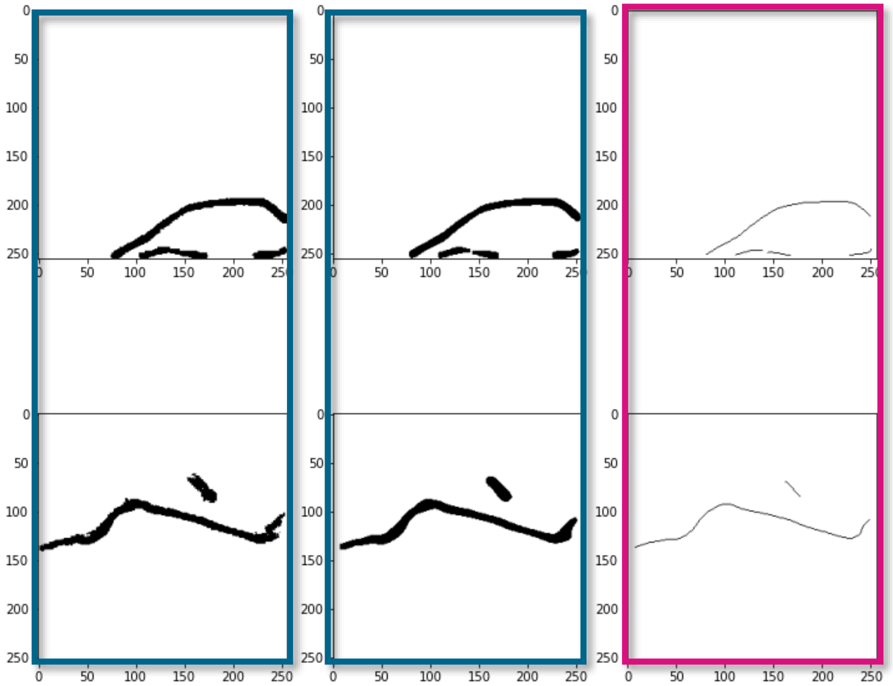

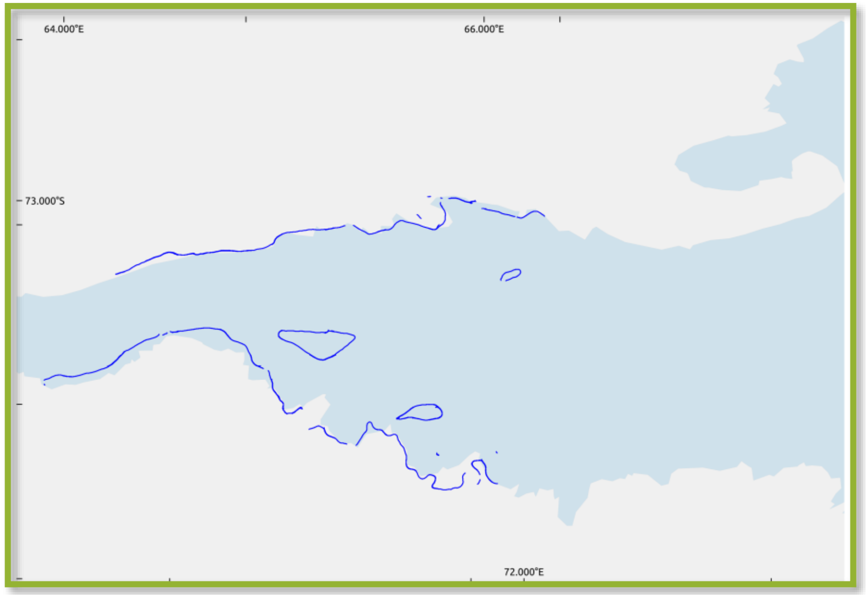

Results

Feature subset	Median deviation [m]	Median Absolute Deviation [m]
DInSAR + DEM + ice velocity	**176.29**	**110.75**
DInSAR + DEM	358.09	232.82
DInSAR + ice velocity	340.46	300.90
DInSAR	188.70	114.84

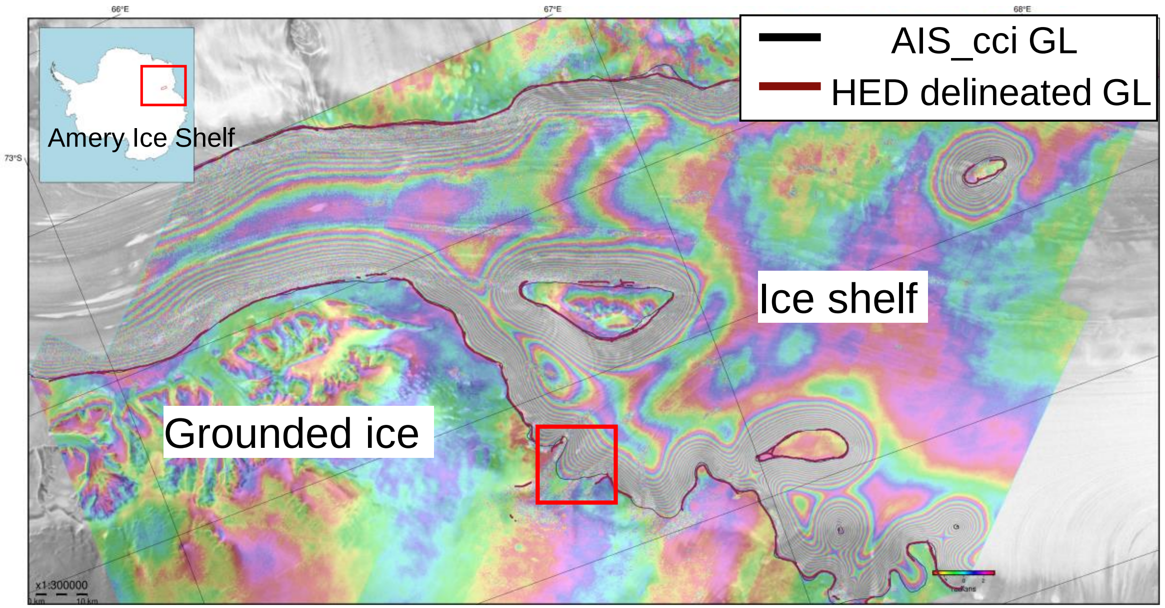

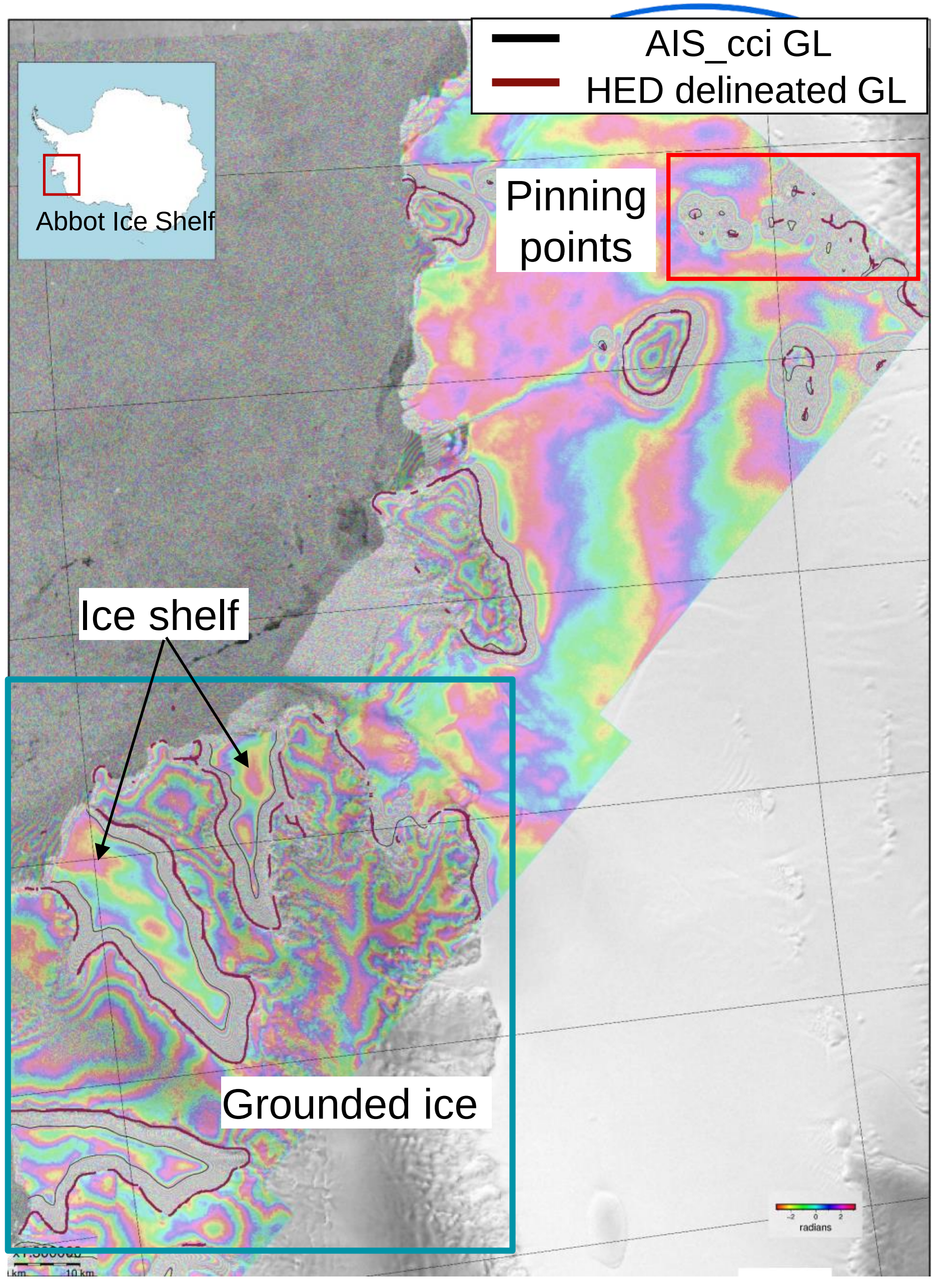

Results

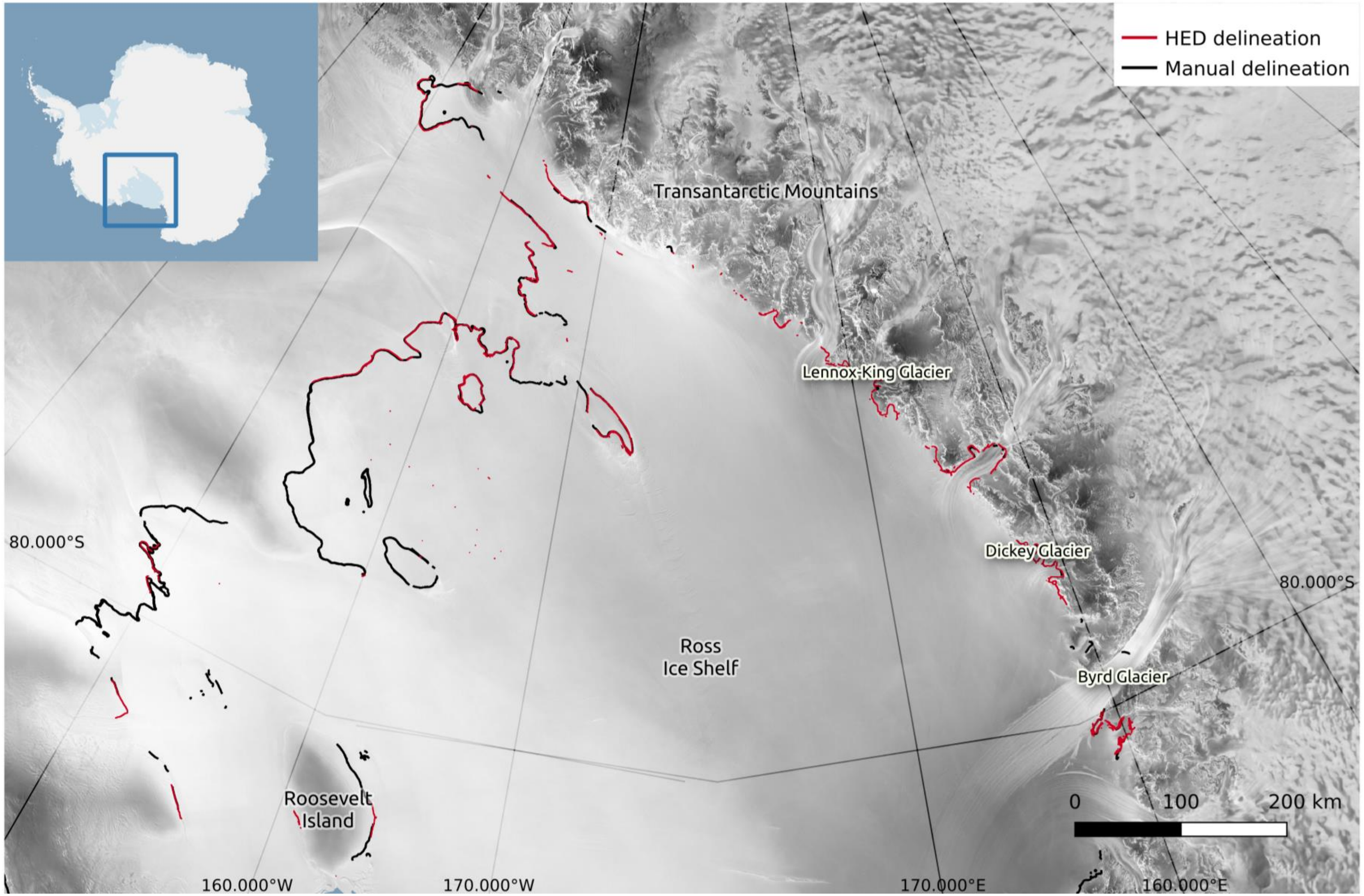
HED delineation
Manual delineation
Transantarctic Mountains
Lennox-King Glacier
Dickey Glacier
Byrd Glacier
Ross
Ice Shelf
Roosevelt
Island
80.000°S
80.000°S
160.000°W
170.000°W
170.000°E
160.000°E
0
100
200 km

Results

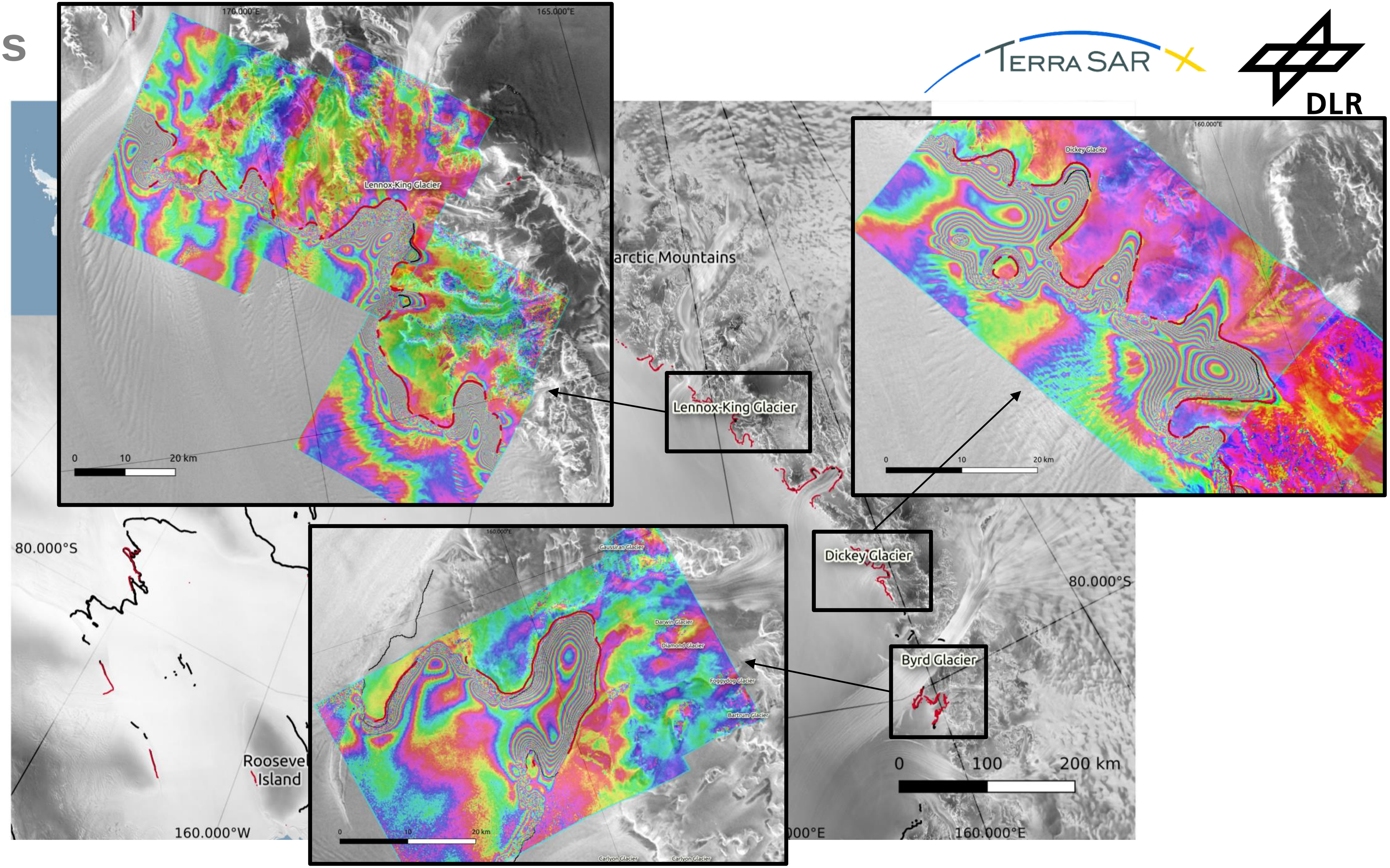
170.000°E
165.000°E
Lennox-King Glacier
0
10
20 km
arctic Mountains
Lennox-King Glacier
160.000°E
Dickey Glacier
0
10
20 km
Dickey Glacier
80.000°S
Byrd Glacier
0
100
200 km
80.000°S
Roosevel
Island
160.000°W
000°E
160.000°E
160.000°E
Gaussiran Glacier
Darwin Glacier
Diamond Glacier
Foggydog Glacier
Bartrum Glacier
0
10
20 km
Carlyon Glacier
Carlyon Glacier

Summary and conclusion

- We developed an end-to-end pipeline for automatic grounding line delineation in DInSAR interferograms
- The quality of the automatically delineated lines is quantified by the low median deviation of **176.29 m** that is achieved by the best performing model
- The DEM and ice velocity do not significantly contribute towards the network performance
- The network fails to delineate interferograms where the fringes are decorrelated
- The pipeline automatically delineates one double difference in the order of seconds → possible to efficiently delineate grounding lines over large areas of the Antarctic Ice Sheet

Phase preserving resampling

(a) Original interferogram, wrapped phase

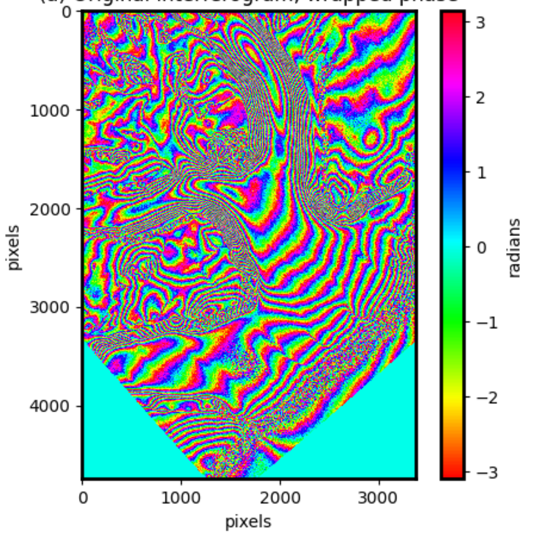

(b) Added unit amplitude

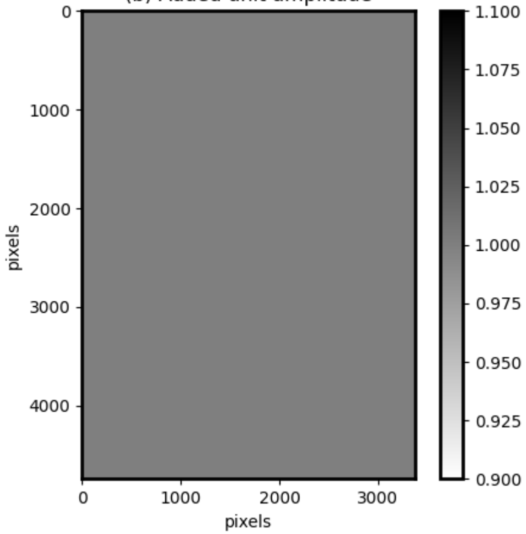

(e) Resampled real component

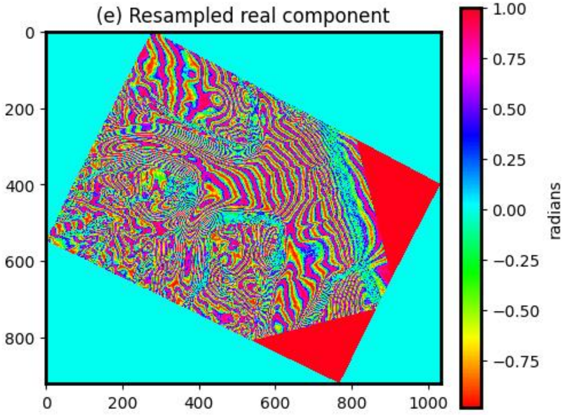

(f) Resampled imaginary component

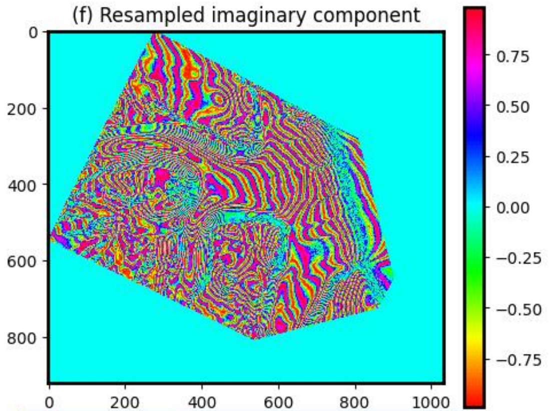

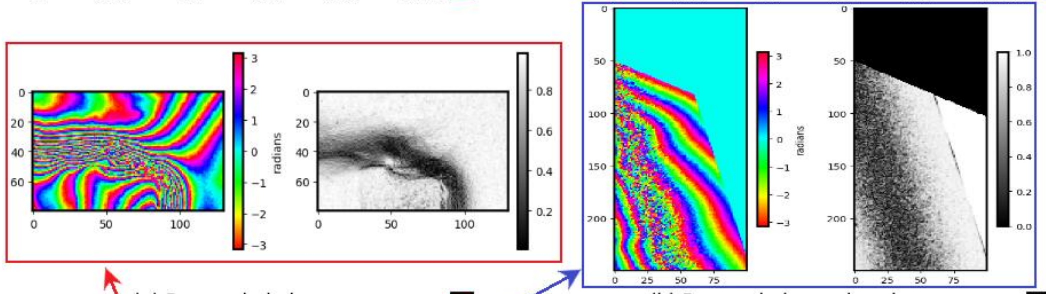

(c) Real component of interferogram

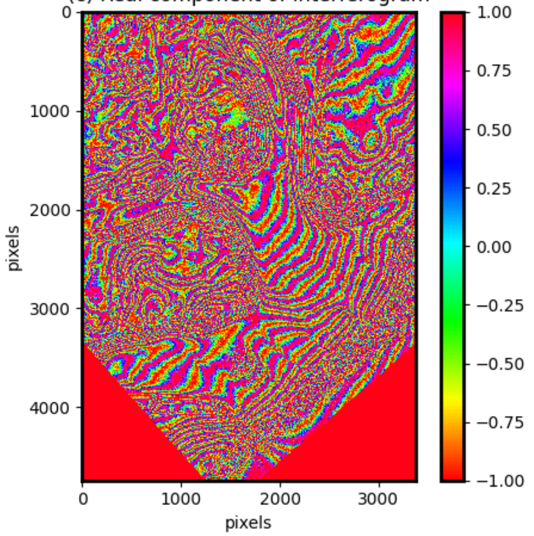

(d) Imaginary component of interferogram

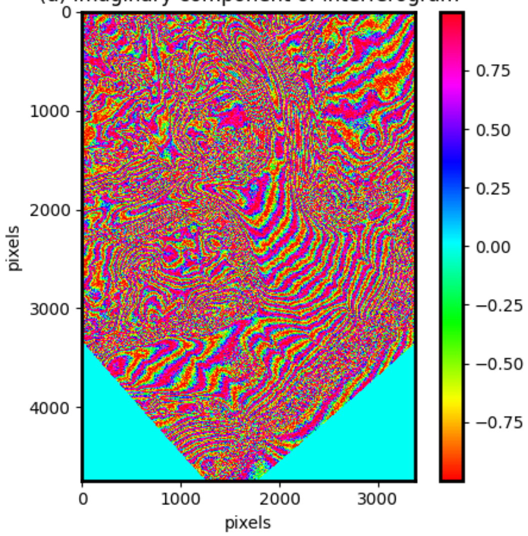

(g) Resampled phase

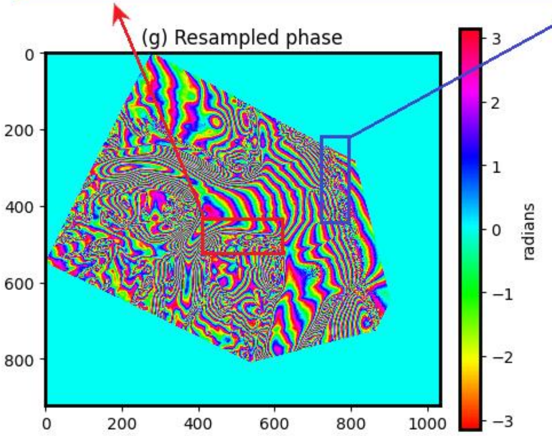

(h) Resampled pseudo coherence

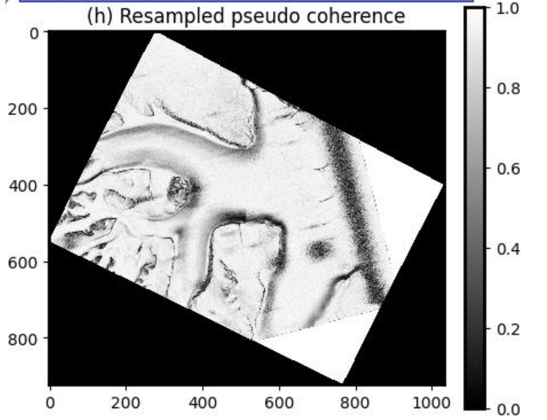

Metrics

Deviations between predicted and manual delineations were quantified with the PoLiS (a metric for polygons and line segments)

$$p(A,B) = \frac{\vec{p}(A,B)}{2q} + \frac{\vec{p}(B,A)}{2r}$$

where $\vec{p}(A,B) = \sum_{a_j \in A}^{q} \min_{b_k \in \partial B} \|a - b\|$

$a_j \in A, j = 1,2,\ldots..q,\ \ b_k \in B, k = 1,2\ldots.r$

∂B are the points on B that are closest to a_j

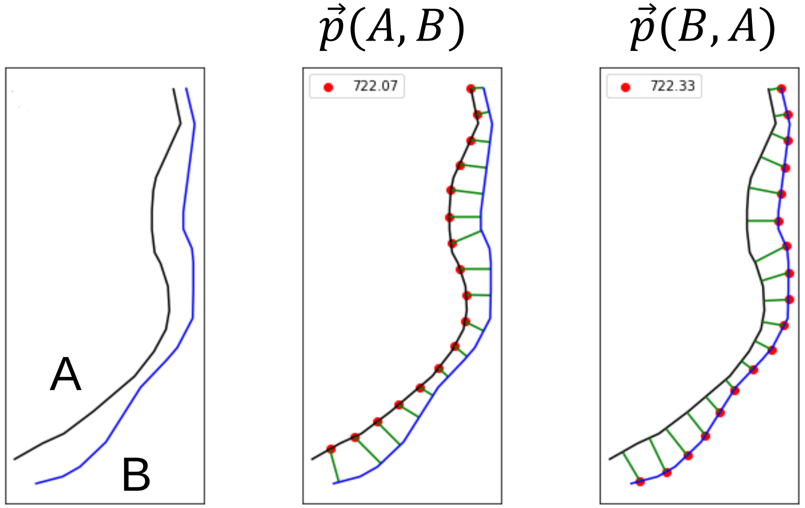

A and B similar in shape and length
→ $\vec{p}(A,B) \approx \vec{p}(B,A)$

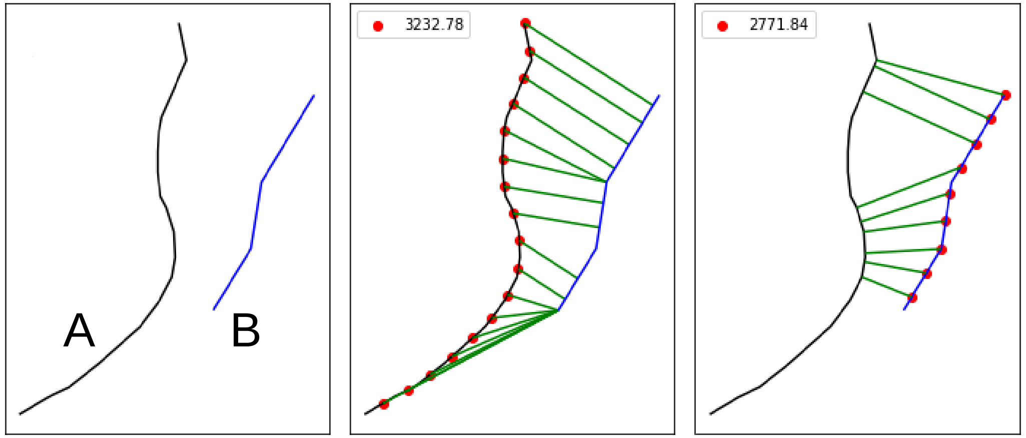

A and B dissimilar in shape and length
→ $\vec{p}(A,B) \neq \vec{p}(B,A)$

Avbelj, J., Muller, R., & Bamler, R. (2015). A Metric for Polygon Comparison and Building Extraction Evaluation. *IEEE Geoscience and Remote Sensing Letters*, *12*(1), 170–174. https://doi.org/10.1109/LGRS.2014.2330695

Dataset split

No. of training samples = 3636 x 2
No. of validation samples = 91
No. of test samples = 511